Austenite reversion kinetics and stability during tempering of an additively manufactured maraging 300 steel

F. F. Conde[1], J. D. Escobar[2], J. P. Oliveira[3], A. L. Jardini[4], W. W. Bose Filho[1] *J. A. Avila[5]

1. Department of Materials Engineering, University of Sao Paulo (USP), Av. Joao Dagnone, 1100 Jd. Sta Angelina, 13563-120, Sao Carlos, Brazil.
2. Metallurgical and Materials Engineering Department, University of São Paulo, 10 Av.Prof. Mello Moraes 2463, 05508-030 São Paulo, SP, Brazil.
3. UNIDEMI, Department of Mechanical and Industrial Engineering, NOVA School of Science and Technology, NOVA University Lisbon, 2829-516 Caparica, Portugal
4. National Institute of Biofabrication (BIOFABRIS), Faculty of Chemical Engineering, State University of Campinas, Av. Albert Einstein 500, 13083-852 Campinas, SP, Brazil.
5. São Paulo State University (UNESP), Campus of São João da Boa Vista, Av. Profª Isette Corrêa Fontão, 505, Jardim das Flores, 13876-750 - São João da Boa Vista, SP, Brazil.

- ***Corresponding author**: * Prof. Dr. Julian A. Avila D. julian.avila@unesp.br, +55 19 36382432, Av. Profª Isette Corrêa Fontão, 505, Jardim das Flores, 13876-750 - São João da Boa Vista, SP, Brazil.

- **Disclosure statement:** No potential conflict of interest was reported by the authors.

Abstract

Reverted austenite is a metastable phase that can be used in maraging steels to increase ductility via transformation-induced plasticity or TRIP effect. In the present study, 18Ni maraging steel samples were built by selective laser melting, homogenized at 820 °C and then subjected to different isothermal tempering cycles aiming for martensite-to-austenite reversion. Thermodynamic simulations were used to estimate the inter-critical austenite + ferrite field and to interpret the results obtained after tempering. In-situ synchrotron X-ray diffraction was performed during the heating, soaking and cooling of the samples to characterize the martensite-to-austenite reversion kinetics and the reverted austenite stability upon cooling to room temperature. The reverted austenite size and distribution were measured by Electron Backscattered Diffraction. Results showed that the selected soaking temperatures of 610 °C and 650 °C promoted significant and gradual martensite-to-austenite reversion with high thermal stability. Tempering at 690 °C caused massive and complete austenitization, resulting in low austenite stability upon cooling due to compositional homogenization.

Keywords: Maraging 300; martensite-to-austenite reversion; additive manufacturing.

1. Introduction

Maraging steels are highly alloyed steels with a low carbon content which exhibit excellent mechanical resistance, combined with good toughness and ductility [1–6]. The austenite-to-martensite transformation in maraging steels contrasts sharply with that of conventional steels, since its low carbon content results in a tough and ductile martensite [1,2,4–6]. The main strengthening mechanism of maraging steels occurs during appropriate aging heat treatments, causing precipitation of intermetallic phases such as Fe_2Mo, Fe_7Mo_6, Ni_3Ti and NiAl , providing a tensile strength above 1500 MPa [1–6].

With the introduction of additive manufacturing (AM) technologies, several iron-based powders started to be used for the production of engineering parts [7–9]. Maraging steel metal powder has been used in laser-based AM since its low carbon content helps to prevent thermal cracking upon cooling [10–12]. Additionally, the as-built AM parts present high strength and hardness, representing potential applications in the injection mold and cutting tool industries, for example [9,12].

Generally, the high strength of the AM parts comes at the expense of ductility and toughness. Before full implementation of AM-based technologies to obtain complex shaped parts, it is necessary to guarantee combinations of ductility, toughness and strength, similar to those obtained via conventional manufacturing routes. One way to increase ductility and toughness in the fabricated AM parts is by applying appropriate post-built heat treatments. However, conventional heat treatment routes need to be carefully reviewed due to the compositional inhomogeneities present in the as-built condition.

Recent studies have focused on the martensite-to-austenite reversion phenomena in maraging steels produced by conventional manufacturing processes. Results led to the improvement of ductility, toughness and strain hardening, yet maintaining very high yield and tensile strengths [13–15] by triggering the TRIP (transformed-induced plasticity) effect. Wang *et al.* [14] studied the tensile strength and Charpy impact toughness in the as-quenched condition and after aging for one and eight hours at 600 °C. Results showed an elongation of 2.4 %, in the as-quenched condition; and a significant increase to 9.9 and 17.1 %, after one and eight hours of aging, respectively. Additionally, the ductile-to-brittle transition temperature (DBTT) decreased from 9 °C in the as-quenched material to -49 and -76 °C after one hour and eight hours of ageing, respectively. A slight drop in yield strength (~18 %) and ultimate tensile strength (~3 %) was also reported for the eight-hour aged condition [14]. Such mechanical performance was associated to the reverted austenite in the microstructure, where the lowest and highest contents of austenite were obtained for the as-quenched and eight-hour aged conditions, respectively. Raabe *et al.* [15]

performed tensile tests in 9 wt. % Mn and 12 wt. % Mn maraging steels in the as-quenched condition and after aging for 48 hours at 450 °C. Results showed a significant ductility improvement after aging, showing total elongation changes from 6 to 15 % for the 9 wt. % Mn maraging steel; and from 16 to 21% for the 12 wt. % Mn maraging steel [15]. Such improvements were attributed to the martensite-to-austenite reversion.

Ex-situ studies on the martensite-to-austenite reversion phenomena can be time consuming under a trial-and-error approach, which requires several experiments at different times and temperatures. In-situ measurements using correlative synchrotron X-ray diffraction and dilatometry can be a more useful approach since the transformation kinetics can be time resolved [16].

It has been reported that the thermal stability of the reverted austenite depends on the reversion temperature. However, isothermal heat treatments near the beginning of martensite-to-austenite transformation temperature (Ac1) are more effective to produce reverted austenite with high thermal stability when compared to isothermal cycles near temperature of complete austenitization (Ac3) [13–20]. Diffusion of austenite-stabilizing elements towards martensite lath/lath interfaces and previous austenite grain boundaries is the main mechanism for martensite-to-austenite reversion and stabilization in a compositionally homogenized martensitic matrix. Whereas, preferential site-specific reversion can occur at preexisting regions with high concentrations of austenite-stabilizing elements in non-homogenized matrixes [16,21], which can be relevant for additive manufacturing metallurgy.

The aim of this work is to study the inter-critical martensite-to-austenite reversion phenomena for samples of maraging 300, produced by selective laser melting. Thermodynamic calculations, electron backscattered diffraction (EBSD) and in-situ synchrotron X-ray diffraction were used. These results are helpful for understanding the effect of non-conventional production technologies, such as additive manufacturing, on the transformation kinetics, thermal stability, morphology and distribution of reverted austenite.

2. Experimental Procedure

2.1. Alloy synthesis

A maraging 300 powder alloy was processed via selective laser melting powder bed fusion technology, using an EOS M280 SLM manufacturing device. The maraging steel powder used as raw material presented a particle size ranging from 40 to 50 μm. The laser power was varied between 180 to 200 W, while the layer thickness was kept constant at 50 μm. The beam spot diameter ranged from 100 to 120 μm [22]. The

chamber was purged with argon before the build-up process to prevent oxidation. Since this technique creates a segregated cellular microstructure, the as-built material was homogenized following recommendations existing in the literature (T>815°C) [1]. The density of the as-built parts was calculated through the Archimedes principle, following the ASTM 962 standard [23]. The material chemical composition was measured by optical emission analysis using an RL-4460 Thermo Fisher, and the carbon and sulfur contents were analyzed by a LECO CS844.

2.2. Thermo-Calc® simulations

Thermodynamic calculations were conducted using Thermo-Calc® software and TCFE8 database. The austenite + ferrite inter-critical region was calculated to determine different isothermal transformation temperatures for martensite-to-austenite reversion. As martensite in maraging steels has a very low carbon content, it can be assumed as ferrite for equilibrium calculations [19,21]. Equilibrium phase diagrams, phase mole fractions and phase compositions were retrieved as a function of temperature and the Ni content.

2.3. In-situ synchrotron analysis

In-situ measurements were performed at the Brazilian National Synchrotron Light Source (LNLS) involving the heating, soaking and cooling of samples using the X-Ray scattering and thermomechanical simulation experimental station (XTMS). The beam energy used was 12 keV (corresponding to a wavelength of 1.035 Å), while the beam size was controlled by slits and set to 0.5 mm height and 2.0 mm wide. A linear detector was used to simultaneously collect diffraction data from a partial spectral region, in a 2θ window varying from 27.9 ° to 37.8 °, which sequentially included the {111}γ, {110}α, and {200}γ families of planes. Dog-bone type samples were used to simulate the tempering cycles. The length of each sample was of 85 mm with a reduced section of 6 mm at the center, and a thickness of 1.8 mm. X-ray diffraction experiments were performed in reflection mode, while simultaneously collecting volumetric responses by a non-contact laser dilatometer (LD). The thermal simulations were performed based on a controlled Joule heating method, where an electric current is applied through the sample producing resistive heat. Type K thermocouples were welded to the samples to control the temperature, with an uncertainty of approximately ±1 K. Prior to testing, all samples were homogenized at 820 °C for one hour and then polished to a mirror-like condition to obtain surfaces suitable for X-ray diffraction.

For austenite thermal reversion, isothermal heat treatments were applied with target temperatures of 610 °C, 650 °C and 690 °C and a constant soaking time of 2200

s as in Figure 1a. The heating rate was 500 °C·s^{-1} to avoid early martensite-to-austenite reversion or intermetallic formation. High heating rate was set to minimize phase transformations and diffusion of alloying elements during the heating stage. The programmed temperature and measured temperature through K thermocouple presented the same behavior for all conditions, as depicted in Figure 1b for the thermal cycle at 900°C. The ultra-fast heating methodology is useful to study the influence of a current compositional distribution on the isothermal austenite reversion kinetics. If the matrix is compositionally homogeneous, austenite reversion will occur towards the thermodynamic equilibrium [24]. Otherwise, meta-equilibrium transition states and site-specific austenite nucleation can occur due to the compositional heterogeneities [21,25]. The cooling rate was 5 °C·s^{-1}, simulating air cooling. During the isothermal plateau and cooling stages, data was acquired every 10 s and 2 s, respectively. A thermal resolution of 10 °C upon cooling was obtained. An extended X-ray diffraction scan was performed for a 2θ range from 20 to 120 ° for all three heat treatment conditions. These extended X-ray diffraction patterns were measured before heating, at the end of the isothermal stage and after cooling.

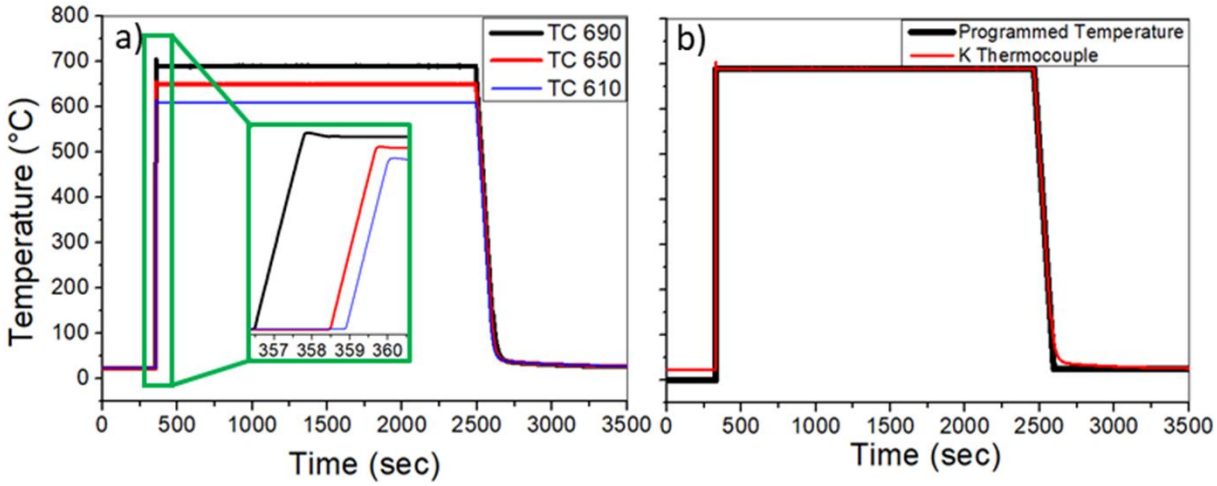

Figure 1. Measured and programmed temperature function diagram of heat treatment process for martensite-to-austenite reversion in the thermomechanical simulator, a) K thermocouple measured temperatures for 690, 650 and 610 °C heat treatments, revealing heating rate of 500 °C·s-1; b) comparison of the programmed temperature and measured temperature through K thermocouple at the 690°C thermal cycle.

Phase fractions were quantified using Equation 1 and Equation 2, which consider the effect of the area under the diffracted peaks, the structure and multiplicity factors for each peak and each phase in the measured volume. In these equations, F_p is the phase fraction of phase p, n_p is the number of peaks from phase p, K represents

a given {hkl} family, A_{pK} is the area below a peak for family K on phase p and R_{pK} is a dimensionless scalar containing the effects of the remaining parameters such as the volume of the unit cell of phase p (V_p), the phase structure factor (f_k) and multiplicity factors (M_k) for each family of planes [26].

$$F_p = \frac{\frac{1}{n_p}\sum_K^{n_{pK}}\frac{A_{pK}}{R_{pK}}}{\sum\frac{1}{n_p}\sum_K^{n_{pK}}\frac{A_{pK}}{R_{pK}}} \quad \text{Equation 1}$$

$$R_{pK} = \frac{{f_k}^2 \cdot M_k}{{V_p}^2} \quad \text{Equation 2}$$

2.4. Microstructural characterization

Samples were ground from 80 to 1200-grit SiC emery paper, polished with CrO 12 µm to 3 µm and polished in silica suspension with 0.06 µm particle size according to the ASTM E3 standard [27]. Etching was performed with 2 % HNO_3 mixed with ethanol for 10 seconds. A FEI Quanta 650 FEG microscope operating at 20 keV was used for electron back-scattered diffraction (EBSD) analysis. EBSD measurements were performed on etched samples with a step size of 0.125 µm. Scanning electron microscopy (SEM) was used for detailed microstructural characterization.

3. Results

3.1. Alloy synthesis

A relative density of 99.19 ± 0.13 % of the as-built parts was achieved compared to wrought counterparts. The measured material chemical composition, depicted in Table 1, was in accordance with the MIL-S-46850D specification [20].

Table 1. Chemical composition (wt. %) of maraging 300 alloy.

Ni	Co	Mo	Ti	Al	C	Mn	Si	V	Fe
18.3	9.2	5.15	0.51	0.056	0.004	0.05	0.11	0.15	Bal.

3.2. Microstructural characterization

The as-built samples showed a typical morphology of weld pool tracks, as depicted in Figure 2 a) to d), with a cellular morphology [28–30]. The presented melt pool profile is composed of a mixture of submicron morphologies, such as dendritic, columnar and cellular, which are typical of AM in steels. This is caused by constitutional supercooling, solute segregation, Marangoni convection and fast solidification conditions [31,32]. As depicted in Figure 2 d), the microstructure presents no preferential crystallographic orientation, which can be attributed to the laser rotation during deposition of new layers, altering the heat flow conditions and consequently the crystal growth direction, as described in the literature [33].

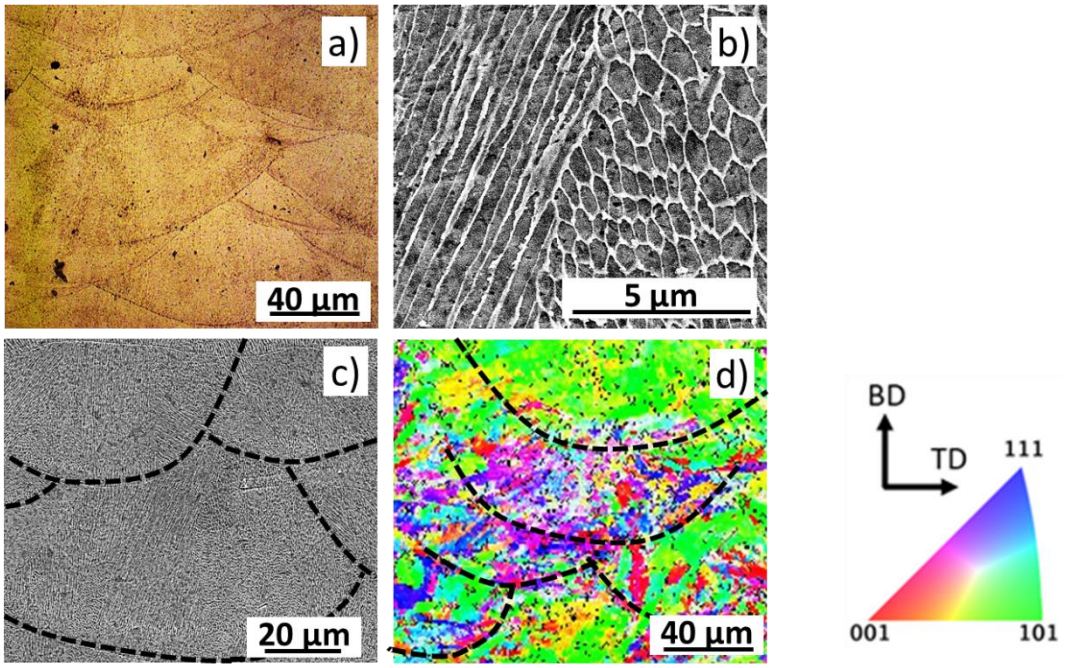

Figure 2. Microstructural characterization of a maraging 300 alloy after selective laser melting: a) optical microscopy characterization; b) SEM micrography of the as-built microstructure; c) SEM micrography of the weld pool-like tracks indicated as black dotted lines; d) EBSD Inverse pole figure. BD: built direction; TD: Transversal direction.

Figure 3 a) shows the effect of homogenization at 820 °C during one hour, which promoted complete austenitization. In this condition, partial recrystallization and grain growth occurred. However, part of the weld tracks and columnar morphologies remained, presenting non-continuous cell boundaries. Figure 3 b), c) and d) present the microstructures after inter-critical tempering at 610, 650 and 690 °C during 2200 s. Partial austenitization occurred at 610 and 650 °C, promoting grain refinement, assisting the dissolution of the columnar features. At 690 °C, complete austenitization

was observed, also promoting grain refinement when compared to the as-built condition. Figure 3 e) shows an EBSD phase map for the inter-critical tempering at 690 °C during 2200 s, revealing reverted austenite in red with a globular morphology.

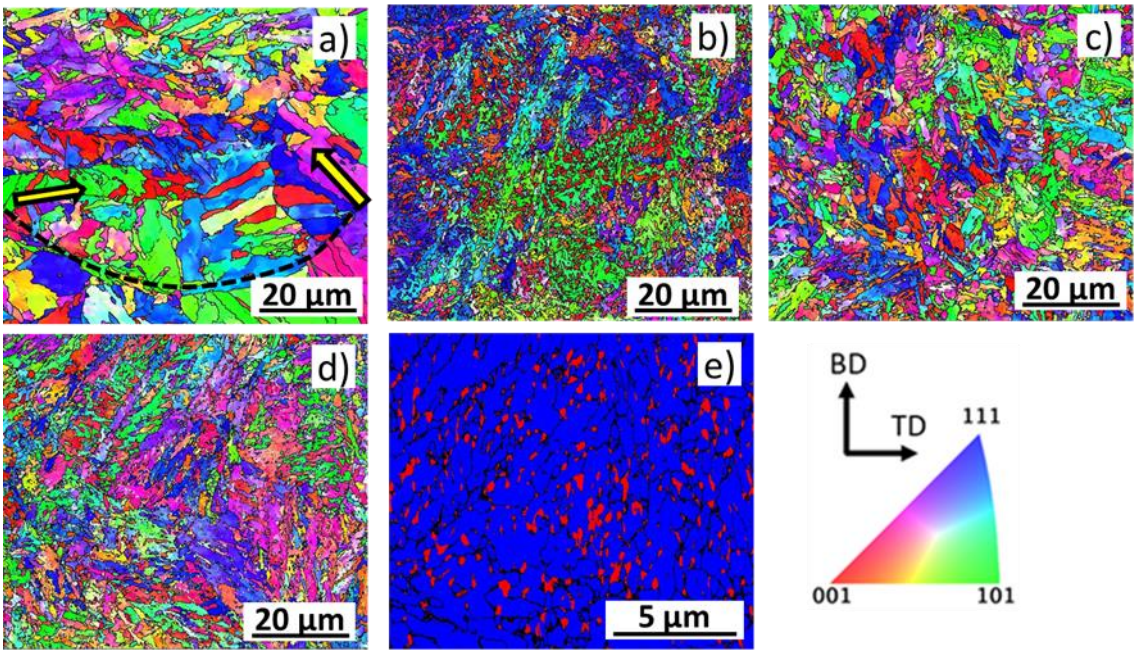

Figure 3. Inverse Pole Figure maps of the microstructures of AM maraging 300 steel after: a) homogenization at 820 °C during one hour; b) tempering at 610 °C during 2200 s; c) tempering at 650 °C during 2200 s; d) tempering at 690 °C during 2200 s. An EBSD phase map of condition d) is presented in e). The yellow arrows in a) indicate reminiscent columnar morphologies. BD: built direction, TD: Transversal direction

3.3. Thermo-Calc® simulations

Figure 4 a) shows the calculated phase diagram according to the nominal composition shown in Table 1. The phase diagram was constructed as a function of temperature and the Ni content, since this is the main element controlling the martensite-to-austenite reversion kinetics and stability for the present case. The dashed vertical line represents the homogenized nominal content of Ni of 18.3 wt. %. If the heat treatment conditions were enough to reach the equilibrium state, a microstructure composed of ferrite (α) + austenite (γ) + μ + Ni_3Ti + TiC can be expected at 610. At 650 °C, Ni_3Ti dissolves and the equilibrium microstructure corresponds to α + γ + μ + TiC. Whereas, according to the thermodynamic simulations, complete austenitization is expected to occur at 690 °C, accompanied by a very small fraction of TiC. This can be observed in detail in Figure 4 b).

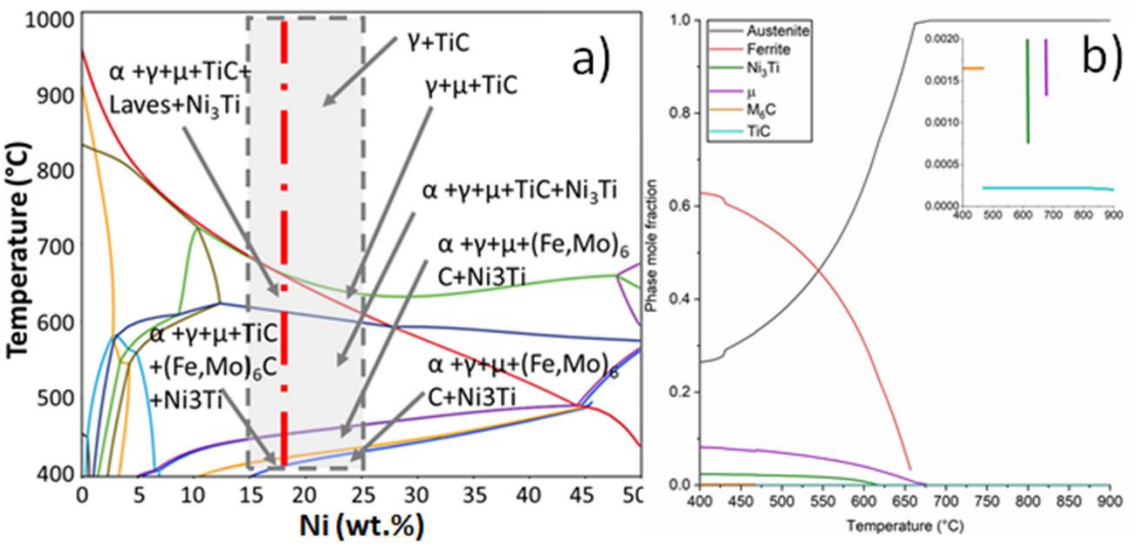

Figure 4. a) Calculated equilibrium phase diagram. The vertical red line in a) indicates the nominal Ni content of 18.3 wt. %. The gray rectangle was drawn to facilitate the visualization of the phases of interest. b) mole fraction of all equilibrium phases calculated for the nominal Ni content as a function of temperature.

Figure 5 exhibits the partitioning of elements in the austenitic phase as a function of temperature. It can be observed that Ni is the main austenite stabilizer element. Above 662 °C, there is no further change in the austenite composition, indicating the dissolution of the described phases except for TiC, which starts decomposing above 830 °C. Thus, heating above 662 °C leads to the formation austenite with the alloy nominal composition. This condition is undesired because no elemental partitioning will occur, strongly compromising the austenite thermal stability upon cooling [21]. However, it is important to highlight that these simulations are only an approach since they are based on equilibrium conditions. Laser-based AM processes, in opposition, have non-equilibrium solidification conditions which often cannot be represented by conventional thermodynamic simulations. Additionally, experimental results shown in Figure 6 and 7 evidence complete austenitization only for the reversion temperature of 690 °C.

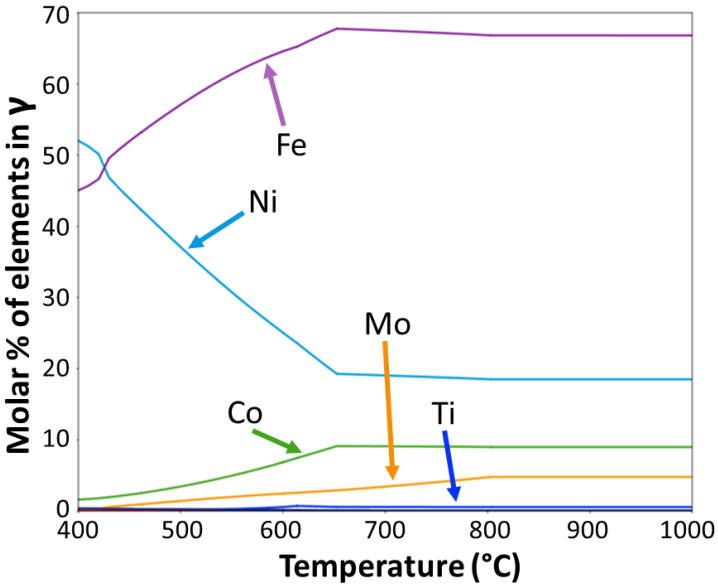

Figure 5. Element partitioning temperature dependence for 18Ni austenite phase.

3.4. In-situ synchrotron: α' → γ isothermal reversion analysis

Figure 6 depicts the in-situ time-resolved X-ray diffraction spectra from 2θ angles between 28 ° and 38 ° for the three tempering conditions, followed by cooling to room temperature. The main peaks covered were {111}γ, {110}α, and {200}γ at approximately 2θ values of 29.0 °, 29.8 °, and 33.6 °, respectively. The diffraction peaks are slightly shifted to the left for increased isothermal transformation temperatures due to the expansion of the unit cells. In this plot, the baseline corresponds to the beginning of the isothermal stage. The blue dash-dot line indicates the separation between the end of the soaking period of 2200 s and the starting of the cooling stage. For 610 °C and 650 °C there is a gradual austenite-to-martensite reversion process, as seen by the reduction of the intensity of the {110}α peak. During cooling, there is a gradual shift of all peaks to higher 2θ values due to thermal contraction. At 690 °C, massive martensite-to-austenite reversion occurred with no noticeable kinetics, at least within the first 10 seconds of exposure time for the first XRD data acquisition. However, almost complete martensitic transformation occurred upon cooling.

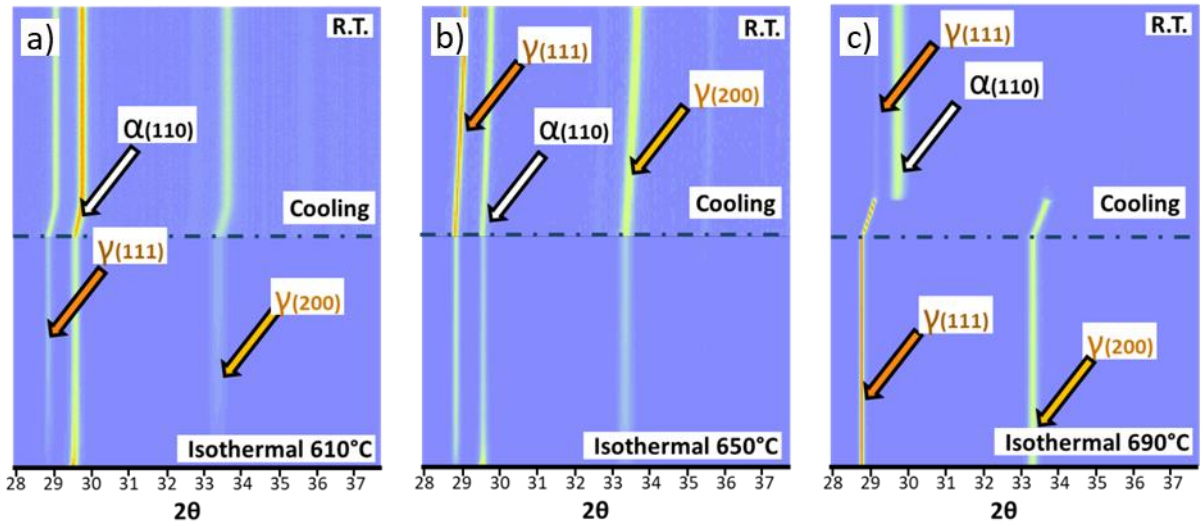

Figure 6. Time resolved synchrotron X-ray diffraction characterization during the simulation of inter-critical tempering cycles at: a) 610 °C; b) 650 °C; c) 690 °C. R.T.: Room Temperature.

Figure 7 shows the correlative results from austenite phase quantification via synchrotron X-ray diffraction (red) and laser dilatometry (black) during the isothermal stage. Tempering at 610 °C resulted in 48 % martensite-to-austenite reversion, the lowest percentage in volume, as expected, after 2200 s. At 650 °C, an austenite volume percentage of 74 % was obtained at the end of the isothermal stage. The slight increasing slopes at 610 and 650 °C indicate that the transformation is unfinished for such tempering time. From the thermodynamic simulations, complete austenitization would occur at approximately 662 °C. In fact, tempering at 690 °C resulted in complete austenitization. Therefore, tempering cycles at 690 °C are not recommended for the reversion of stable austenite. For all conditions, contraction of the sample was observed by LD and was related to the martensite-to-austenite reversion. A very fast contraction was observed at 690 °C, along with immediate austenitization by synchrotron x-ray diffraction, indicating a massive reversion mechanism. Some additional volumetric expansion was detected at 650 and 690 °C. This effect can be related to several possible factors, such as compositional redistributions, precipitation of intermetallic phases and minor surface oxidation, which are not the scope of this work.

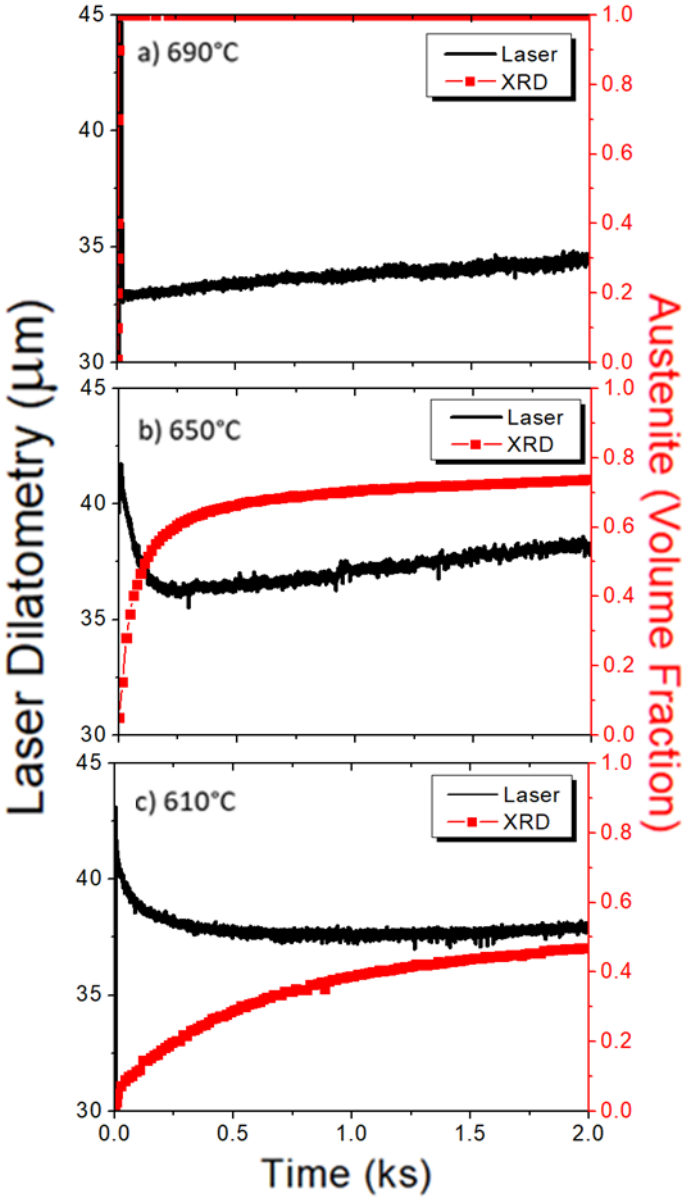

Figure 7. Martensite-to-austenite reversion kinetics observed by synchrotron X-ray diffraction combined with laser dilatometry for the isothermal tempering temperatures of: a) 690 °C; b) 650 °C; c) 610 °C. In all cases, the soaking time was set to 2200 s.

3.5. Reverted γ stability upon cooling

Results from synchrotron X-ray diffraction along the isothermal and cooling stages are presented in Figure 8 as a function of time. The austenite thermal stability can be viewed as the amount of austenite-to-martensite transformation upon cooling. Although complete martensite-to-austenite reversion occurred at 690 °C, only a volumetric percentage of 10 % remained stabilized after cooling to room temperature. This type of austenite can be associated to a retention process, most likely due to local

segregation of Ni. However, almost all austenitic grains underwent compositional homogenization, strongly reducing the relative thermal stability. Nevertheless, compositional inhomogeneities due to incomplete solubilization of austenite-stabilizing elements could have remained, resulting in local austenite retention. The isothermal tempering at 650 and 610 °C produced final austenite percentages of 74 and 48 %, respectively. After cooling, a slight martensitic transformation of approximately 2 % could be measured for the tempering temperature of 650 °C. Whereas, no martensitic transformation occurred after tempering at 610 °C.

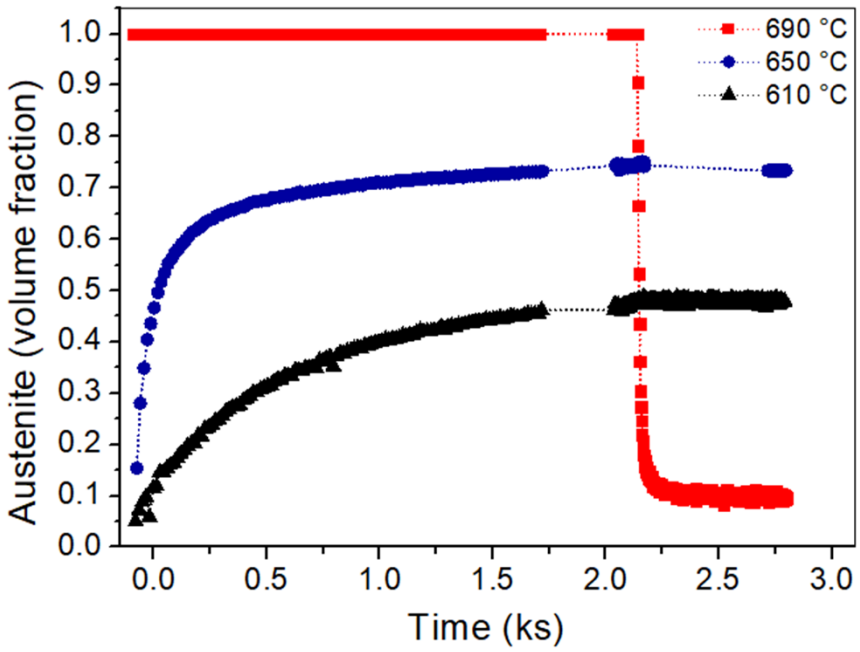

Figure 8. In-situ synchrotron X-ray diffraction analysis for the isothermal martensite-to-austenite reversion kinetics and its thermal stability during cooling.

4. Discussion

In the present work, three isothermal tempering temperatures were used to verify the martensite-to-austenite reversion process and the austenite thermal stability upon cooling after selective laser melting and solubilization. To trigger the martensite-to-austenite reversion, it is necessary to heat the material between Ac1 and Ac3. Usually, maraging 300 alloys can be homogenized at temperatures above 815 °C [1], which is far from the calculated austenitization temperature in thermodynamic equilibrium of 662 °C, known as Ae3. Nevertheless, EBSD results evidenced that the

homogenization cycle at 820 °C during one hour was still not sufficient to erase all AM typical features, such as cellular and columnar morphologies.

All three isothermal treatments were effective to significantly reduce the grain size when compared to the solubilized condition. Inter-critical tempering cycles result in the martensite-to-austenite reversion at the martensite lath, block and packet interfaces by diffusion-controlled reactions, promoting grain refinement [2,34]. The reverted austenite can appear as acicular or globular shapes depending on the heating rate and the tempering temperature [35–37]. Acicular laths form at the lower portion of the inter-critical field upon slow heating rates. The globular austenite forms at the higher portion of the inter-critical field and upon fast heating rates and preferentially forms at the boundary of the martensite packets or at the prior austenite grain boundary [35,36]. In both cases, the incomplete reversion process can lead to refinement of the microstructure [35,36]. Another advantage of grain refinement caused by the martensite-to-austenite reversion is that there are more grain boundaries acting as topological obstacles for crack propagation [38,39]. In the present work, a fast heating rate of 500 $°C \cdot s^{-1}$ was used, and the reversion temperatures were way above the expected Ae1 temperature, causing the formation of a reverted austenite mainly with globular morphologies.

Equilibrium calculations for 610 and 650 °C predicted the coexistence of austenite and ferrite, along with precipitates such as μ, TiC and Ni_3Ti, where the latter dissolves slightly above 610 °C. Through synchrotron X-ray diffraction analyzes, it is difficult to determine the presence of small quantities of those precipitates. However, its presence cannot be disregarded [1,40,41]. On the other hand, calculations predicted complete austenitization at 662 °C. Experimental results revealed complete austenitization only at 690 °C.

Martensite-to-austenite reversion may occur by a displacive or diffusive process [42–44], and such mechanisms strongly depend on the heating rate and transformation temperature [42,43]. The martensite-to-austenite reversion reaction is energetically favored as it passes through the equilibrium austenite transformation start temperature Ae1, separating the stability ranges of the two phases [44]. Above this temperature, the free energy of the system is reduced when the product phase (austenite with a lower free energy) transforms from the parent phase (ferrite with a higher free energy). This free energy reduction is a function of the transformation temperature, which determines the total equilibrium fraction of the product phase [44]. Additionally, the compositional strains for martensite-to-austenite reversion are also dictated by temperature.

Martensite-to-austenite reversion and austenite stabilization at room temperature were studied in modified maraging steels [15,18–20]. It has been reported that there is a change in composition at the martensite-austenite interface and a phase

boundary motion towards martensite in detriment of austenite growth [19,20]. Locally, there is a diffusion-controlled process of segregation of austenite stabilizer elements into the formed austenite islands when the steel is heated between Ac1 and Ac3. As time is prolonged, more elements such as Ni and Mn will segregate, producing a more stable austenite locally. For slow heating rates, the diffusive mechanism is favored and significant segregation of austenite-stabilizing elements can occur at the martensite grain boundaries and lath/lath interfaces. Provided enough time, partitioning will occur, promoting a matrix with nickel-rich and nickel-depleted regions, which will eventually lead to martensite-to-austenite reversion [16,42,43]. From Figure 5, it can be inferred that the partitioning of Ni into the reverted austenite at 610 °C was stronger than that at 650 °C. As a consequence, a martensitic transformation of 2 % was found after cooling from 650 °C. Whereas, no martensitic transformation occurred when cooled from 610 °C, as presented in Figure 8.

As shown in Figure 5, the higher the temperature, the lower the Ni partitioning necessary for martensite-to-austenite reversion. Therefore, the massive reversion mechanism is favored at the higher portion of the inter-critical field, given the reduced critical Ni for the transformation to occur [36,45]. This is consistent with the observations at 690 °C. As the isothermal soaking temperature approaches Ae3, more austenite is formed and the stabilizing elements are distributed, resulting in reduced thermal stability. Therefore, heating near Ac3 will not be efficient for austenite stabilization as the alloy reaches a near homogenization condition. Such strong stabilizing effect of Ni and its role during the inter-critical martensite-to-austenite reversion is widely discussed in literature [13,15,16,42,46,47].

Regarding the fact that the present alloy was produced by selective laser melting, martensite-to-austenite reversion may have been facilitated since solubilization at 820 °C did not fully recrystallize the AM microstructure. Solubilization cycles at 920 and 980 °C have been observed to produce a more recrystallized grain structure with better dissolution of the as-built microstructure [48]. According to dilatometry measurements, a short solubilization cycle of 820 °C during five minutes actually resulted in incomplete martensitic transformation, i.e., austenite retention [48]. Additionally, a smaller grain size can also lead to a higher density of nucleation sites for austenite reversion [49].

5. Conclusions

The effect of different heat treatment cycles to promote homogenization and significant austenite reversion in a maraging 300 steel produced by selective laser melting was studied. The following main conclusions can be drawn:

- Martensite-to-austenite reversion between 610 and 690 °C under a heating rate of 500 °C·s^{-1} promoted microstructural refinement, compared to the homogenized case, due to the formation of intra-granular acicular and globular austenite morphologies.
- Isothermal tempering heat treatments up to 650 °C are effective to provide martensite-to-austenite reversion with high thermal stability during cooling to room temperature.
- Heat treatment temperatures above Ae3 under very fast heating rate of 500 °C·s^{-1} promoted martensite-to-austenite reversion by a displacive mechanism, resulting in low thermal stability upon cooling due to small partitioning, i.e., homogenization effect.
- There is a loss of capacity to stabilize reverted austenite at room temperature when the tempering temperature exceeds the critical threshold for efficient partitioning, which is expected above 650 °C.
- Despite the homogenization cycle at 820 °C during one hour used to promote complete austenitization, this was not sufficient to erase all the microstructural features typical of additive manufacturing in the as-built condition.
- Thermodynamic calculations provided guidance in determining optimum heat treatment temperatures for the homogenization of precipitates and for martensite-to-austenite reversion with high thermal stability.

Acknowledgments

We would like to thank the Brazilian Nanotechnology National Laboratory (LNNano), CNPEM/MCTIC and Brazilian Synchrotron Light Laboratory (LNLS) CNPEM/MCTIC for the use of the SEM/EBSD and the XTMS beamline, respectively. Authors acknowledge FAPESP (2017/17697-5), FAPESP (2008/57863-0), FAPESP (2014/20844-1) and CNPq (573661/2008-1), Coordenação de Aperfeiçoamento de Pessoal de Nível Superior - Brasil (CAPES) - Finance Code 001. J. P. Oliveira acknowledges Fundação para a Ciência e Tecnologia (FCT) for its financial support through the project UID/EMS/00667/2019. The chemical composition measurements were conducted at VILLARES METALS.

References

[1] ASM, ASM Handbook - Heat Treatment, ASM Handb. 4 (1991) 3470. doi:10.1016/S0026-0576(03)90166-8.

[2] R.F. Decker, J.T.T. Eash, A.J.J. Goldman, 18% Nickel Maraging Steel.pdf,

Trans. ASM. 55 (1962) 58–76.
[3] J.W.M. Jr, Making steel strong and cheap, Nat. Publ. Gr. 16 (2017) 787–789. doi:10.1038/nmat4949.
[4] R.F. Decker, C.J. Novak, T.W. Landig, Developments and projected trends, (n.d.).
[5] A. Kumar, Y. Balaji, N.E. Prasad, Type Certification of 18 Ni Maraging Steels for Landing Gears, Mater. Sci. Forum. 710 (2012) 511–515. doi:10.4028/www.scientific.net/MSF.710.511.
[6] B.-Z. Weiss, Maraging Steels—Structure, Properties and Applications, Pergamon Press Ltd., 1983. doi:10.1016/B978-0-08-029358-5.50009-4.
[7] D. Gu, Laser Additive Manufacturing (AM): Classification, Processing Philosophy, and Metallurgical Mechanisms, 2015. doi:10.1007/978-3-662-46089-4_2.
[8] I. Gibson, D. Rosen, B. Stucker, Additive Manufacturing Technologies, Springer New York, New York, NY, 2015. doi:10.1007/978-1-4939-2113-3.
[9] D. Herzog, V. Seyda, E. Wycisk, C. Emmelmann, Additive manufacturing of metals, Acta Mater. 117 (2016) 371–392. doi:10.1016/j.actamat.2016.07.019.
[10] K. Kempen, L. Thijs, E. Yasa, J. Van Humbeeck, P. Procedia, E. Yasa, Microstructure and mechanical properties of Selective Laser Melted 18Ni300 steel Microstructure and mechanical properties of Selective Laser Melted, Phys. Procedia. 12 (2011) 255–263. doi:10.1016/j.phpro.2011.03.033.
[11] S. Hoeges, Development of a Maraging Steel Powder for Additive Manufacturing, Sinter Met. Eng. (n.d.).
[12] K.J.A.A. Brookes, Maraging steel for additive manufacturing – Philipp Stoll's paper at DDMC 2016, Met. Powder Rep. 71 (2016) 149–152. doi:10.1016/j.mprp.2016.04.087.
[13] M. Wang, C.C. Tasan, D. Ponge, D. Raabe, Acta Materialia Spectral TRIP enables ductile 1 . 1 GPa martensite, Acta Mater. 111 (2016) 262–272. doi:10.1016/j.actamat.2016.03.070.
[14] M. Wang, C.C. Tasan, D. Ponge, A. Dippel, D. Raabe, ScienceDirect Nanolaminate transformation-induced plasticity – twinning-induced plasticity steel with dynamic strain partitioning and enhanced damage resistance, Acta Mater. 85 (2015) 216–228. doi:10.1016/j.actamat.2014.11.010.
[15] D. Raabe, D. Ponge, O. Dmitrieva, B. Sander, Nanoprecipitate-hardened 1.5 GPa steels with unexpected high ductility, Scr. Mater. 60 (2009) 1141–1144. doi:10.1016/j.scriptamat.2009.02.062.
[16] J.D. Escobar, G.A. Faria, L. Wu, J.P.P. Oliveira, P.R.R. Mei, A.J. Ramirez, Austenite reversion kinetics and stability during tempering of a Ti-stabilized supermartensitic stainless steel: correlative in situ synchrotron x-ray diffraction and dilatometry, Acta Mater. 138 (2017) 92–99. doi:10.1016/j.actamat.2017.07.036.
[17] D. Raabe, S. Sandlöbes, J. Millán, D. Ponge, H. Assadi, M. Herbig, P.P. Choi, J. Milla, Segregation engineering enables nanoscale martensite to austenite phase transformation at grain boundaries: A pathway to ductile martensite, Acta Mater. 61 (2013) 6132–6152. doi:10.1016/j.actamat.2013.06.055.
[18] D. Raabe, D. Ponge, O. Dmitrieva, B. Sander, Designing ultrahigh strength steels with good ductility by combining transformation induced plasticity and martensite aging, Adv. Eng. Mater. 11 (2009) 547–555.

543 doi:10.1002/adem.200900061.
544 [19] O. Dmitrieva, D. Ponge, G. Inden, J. Millán, P. Choi, J. Sietsma, D. Raabe,
545 Chemical gradients across phase boundaries between martensite and
546 austenite in steel studied by atom probe tomography and simulation, Acta
547 Mater. 59 (2011) 364–374. doi:10.1016/j.actamat.2010.09.042.
548 [20] M.M. Wang, C.C. Tasan, D. Ponge, A. Kostka, D. Raabe, Smaller is less
549 stable: Size effects on twinning vs. transformation of reverted austenite in
550 TRIP-maraging steels, Acta Mater. 79 (2014) 268–281.
551 doi:10.1016/j.actamat.2014.07.020.
552 [21] J.D. Escobar, J.P. Oliveira, C.A.F. Salvador, G.A. Faria, J.D. Poplawsky, J.
553 Rodriguez, P.R. Mei, S.S. Babu, A.J. Ramirez, Meta-equilibrium transition
554 microstructure for maximum austenite stability and minimum hardness in a Ti-
555 stabilized supermartensitic stainless steel, Mater. Des. 156 (2018) 609–621.
556 doi:10.1016/j.matdes.2018.07.018.
557 [22] EOS GmbH, EOS, Material data sheet EOS Maraging Steel MS1, Eos
558 (Washington. DC). 49 (2011) 6. http://ip-saas-eos-
559 cms.s3.amazonaws.com/public/1af123af9a636e61/042696652ecc69142c8518
560 dc772dc113/EOS_MaragingSteel_MS1_en.pdf.
561 [23] ASTM E962-17, Standard Test Methods for Density of Compacted or Sintered
562 Powder Metallurgy (PM) Products Using Archimedes ' Principle, ASTM B.
563 Stand. (2017) 1–7. doi:10.1520/B0962-17.2.
564 [24] J.D. Escobar, G.A. Faria, E.L. Maia, J.P. Oliveira, T. Boll, S. Seils, P.R. Mei,
565 A.J. Ramirez, Fundamentals of Isothermal Austenite Reversion in a Ti-
566 Stabilized 12cr-6 Ni-2 Mo Super Martensitic Stainless Steels: Thermodynamics
567 Versus Experimental Assessments, Acta Mater. (2019).
568 [25] M. Belde, H. Springer, G. Inden, D. Raabe, Multiphase microstructures via
569 confined precipitation and dissolution of vessel phases: Example of austenite in
570 martensitic steel, Acta Mater. 86 (2015) 1–14.
571 doi:10.1016/j.actamat.2014.11.025.
572 [26] G.A. Faria, Exploring Metallic Materials Behavior Through In Situ
573 Crystallographic Studies by Synchrotron Radiation, (2012) 152.
574 [27] ASTM E3, E3-11 Standard Guide for Preparation of Metallographic Specimens
575 1, ASTM B. Stand. i (2011) 1–12. doi:10.1520/E0003-11.2.
576 [28] Y. Ji, L. Chen, L. Chen, Understanding Microstructure Evolution During
577 Additive Manufacturing of Metallic Alloys Using Phase-Field Modeling, 1st ed.,
578 Elsevier Inc., 2018. doi:10.1016/B978-0-12-811820-7.00008-2.
579 [29] K.G. Prashanth, J. Eckert, Formation of metastable cellular microstructures in
580 selective laser melted alloys, J. Alloys Compd. 707 (2017) 27–34.
581 doi:10.1016/j.jallcom.2016.12.209.
582 [30] J.P. Oliveira, R.M. Miranda, F.M. Braz Fernandes, Welding and Joining of NiTi
583 Shape Memory Alloys: A Review, Prog. Mater. Sci. 88 (2017) 412–466.
584 doi:10.1016/j.pmatsci.2017.04.008.
585 [31] C. Tan, K. Zhou, M. Kuang, W. Ma, T. Kuang, C. Tan, Microstructural
586 characterization and properties of selective laser melted maraging steel with
587 different build directions maraging steel with di ff erent build directions, Sci.
588 Technol. Adv. Mater. 19 (2018) 746–758.
589 doi:10.1080/14686996.2018.1527645.
590 [32] J.P. Oliveira, A.J. Cavaleiro, N. Schell, A. Stark, R.M. Miranda, J.L. Ocana,

F.M. Braz Fernandes, Effects of laser processing on the transformation characteristics of NiTi: A contribute to additive manufacturing, Scr. Mater. 152 (2018) 122–126. doi:10.1016/j.scriptamat.2018.04.024.
[33] J. Suryawanshi, K.G. Prashanth, U. Ramamurty, Tensile, fracture, and fatigue crack growth properties of a 3D printed maraging steel through selective laser melting, J. Alloys Compd. (2017) 1–35. doi:10.1016/j.jallcom.2017.07.177.
[34] S. Floreen, The physical metallurgy maraging steels, Metall. Rev. (1968).
[35] X. Zhang, G. Miyamoto, Y. Toji, S. Nambu, T. Koseki, T. Furuhara, Orientation of austenite reverted from martensite in Fe-2Mn-1 . 5Si-, Acta Mater. 144 (2018) 601–612. doi:10.1016/j.actamat.2017.11.003.
[36] H. Shirazi, G. Miyamoto, S.H. Nedjad, H. Ghasemi-nanesa, M.N. Ahmadabadi, T. Furuhara, Microstructural evaluation of austenite reversion during intercritical annealing of Fe – Ni – Mn martensitic steel, J. Alloys Compd. 577 (2013) S572–S577. doi:10.1016/j.jallcom.2012.02.015.
[37] S.T. Kimmins, D.J. Gooch, Austenite memory effect in 1Cr-1 Mo-O-75V (Ti , B) steel, 17 (1983) 519–532.
[38] A.K. Vasudevan, K. Sadananda, K. Rajan, Role of microstructures on the growth of long fatigue cracks, 19 (1998) 151–159.
[39] J.P. Oliveira, Z. Zeng, T. Omori, N. Zhou, R.M. Miranda, F.M.B. Fernandes, Improvement of damping properties in laser processed superelastic Cu-Al-Mn shape memory alloys, JMADE. 98 (2016) 280–284. doi:10.1016/j.matdes.2016.03.032.
[40] O. Moshka, M. Pinkas, E. Brosh, V. Ezersky, L. Meshi, Addressing the issue of precipitates in maraging steels - Unambiguous answer, Mater. Sci. Eng. A. 638 (2015) 232–239. doi:10.1016/j.msea.2015.04.067.
[41] Z. Guo, W. Sha, D. Li, Quantification of phase transformation kinetics of 18 wt.% Ni C250 maraging steel, Mater. Sci. Eng. A. 373 (2004) 10–20. doi:10.1016/j.msea.2004.01.040.
[42] R. Kapoor, L. Kumar, I.S. Batra, A dilatometric study of the continuous heating transformations in 18wt.% Ni maraging steel of grade 350, Mater. Sci. Eng. A. 352 (2003) 318–324. doi:10.1016/S0921-5093(02)00934-6.
[43] L.G. de Carvalho, M.S. Andrade, R.L. Plaut, F.M. Souza, A.F. Padilha, A Dilatometric Study of the Phase Transformations in 300 and 350 Steels During Continuous Heating Rates, Mater. Res. 16 (2013) 740–744. doi:10.1590/S1516-14392013005000069.
[44] R. Abbaschian, L. Abbaschian, R.E. Reed-Hill, Physical Metallurgy Principles, Fourth Ed., Cengage Learning, 2009.
[45] M. Belde, H. Springer, D. Raabe, Vessel microstructure design: A new approach for site-specific core-shell micromechanical tailoring of TRIP-assisted ultra-high strength steels, Acta Mater. 113 (2016) 19–31. doi:10.1016/j.actamat.2016.04.051.
[46] S.D. Antolovich, A. Saxena, G.R. Chanani, Increased Fracture Toughness in a 300 Grade Maraging Steel as a Result of Thermal Cycling, Metall. Trans. 5 (1974) 623–632.
[47] K. Nakazawa, Y. Kawabe, S. Muneki, Grain Refinement of Austenite through Reverse Transformation from Martensite in Fe-l5Ni-Co-Mo-Ti Alloys, Trans. ISIJ. 23 (1983) 347–356.
[48] F.F. Conde, J.D. Escobar, J.P. Oliveira, M. Béreš, A.L. Jardini, W.W. Bose,

J.A. Avila, Effect of thermal cycling and aging stages on the microstructure and bending strength of a selective laser melted 300-grade maraging steel, Mater. Sci. Eng. A. (2019) 15. doi:10.1016/j.msea.2019.03.129.

[49] A. Bojack, L. Zhao, P.F. Morris, J. Sietsma, Austenite Formation from Martensite in a 13Cr6Ni2Mo Supermartensitic Stainless Steel, Metall. Mater. Trans. A Phys. Metall. Mater. Sci. 47 (2016) 1996–2009. doi:10.1007/s11661-016-3404-z.